Revealing the Topography of Cellular Membrane Domains by Combined Atomic Force Microscopy/Fluorescence Imaging

D. J. Frankel,* J. R. Pfeiffer,† Z. Surviladze,† A. E. Johnson,‡ J. M. Oliver,† B. S. Wilson,† and A. R. Burns*
*Biomolecular Materials and Interfaces Department, MS1413 Sandia National Laboratories, Albuquerque, New Mexico 87185;
†Department of Pathology and Cancer Research and Treatment Center, University of New Mexico, Albuquerque, New Mexico 87131;
and ‡School of Medicine, Texas A&M University, College Station, Texas 77843

ABSTRACT Simultaneous atomic force microscopy (AFM) and confocal fluorescence imaging were used to observe in aqueous buffer the three-dimensional landscape of the inner surface of membrane sheets stripped from fixed tumor mast cells. The AFM images reveal prominent, irregularly shaped raised domains that label with fluorescent markers for both resting and activated immunoglobin E receptors (FcεRI), as well as with cholera toxin-aggregated GM1 and clathrin. The latter suggests that coated pits bud from these regions. These features are interspersed with flatter regions of membrane and are frequently surrounded and interconnected by cytoskeletal assemblies. The raised domains shrink in height by ~50% when cholesterol is extracted with methyl-β-cyclodextrin. Based on composition, the raised domains seen by AFM correspond to the cholesterol-enriched dark patches observed in transmission electron microscopy (TEM). These patches were previously identified as sites of signaling and endocytosis based on their localization of activated FcεRI, at least 10 associated signaling molecules, and the presence of clathrin-coated pits. Overall the data suggest that signaling and endocytosis occur in mast cells from raised membrane regions that depend on cholesterol for their integrity and may be organized in specific relationship with the cortical cytoskeleton.

INTRODUCTION

Models of cell membrane organization are still evolving. Experimental evidence gathered over several decades suggests that the fluid mosaic model (1) fails to fully account for the possibility of ordered domains and other evidence of membrane heterogeneity (2–6). The modern concept that membranes are made up of distinct and dynamic mixtures of ordered and disordered lipid domains is based in part on model membrane studies that dramatically demonstrate phase separation of lipids, due largely to their state of saturation (7,8). Evidence for the partitioning of cholesterol and specific cellular lipids and proteins into ''lipid rafts'' in cells comes principally from their detergent insolubility and subsequent recovery in light fractions of sucrose density gradients (9,10).

Recent evidence from electron microscopy that typical ''raft markers'', such as glycosylphosphatidylinositol (GPI)-anchored proteins and GM1 ganglioside, fail to colocalize either with each other or with signaling receptors confirms the nonrandom topographical organization of native cell membranes and suggests that microdomains may be much more numerous and heterogeneous than suggested from biochemical studies (2,11). Membrane domains may also be much smaller than originally suggested. Several groups have proposed that domains in resting cells are <70 nm in size (12,13). Using laser trapping and single particle tracking (SPT) techniques, Pralle et al. (14) estimated GPI-linked proteins to reside in rafts as small as 26 ± 13 nm in diameter. In transmission electron microscopy (TEM) studies of membrane sheets, Prior et al. (15) found Ras in microdomains of mean radius 22 ± 4 nm. Remarkably, these domains occupied 35% of the plasma membrane.

Immunogold labeling and electron microscopic imaging of endogenous proteins in the cytoplasmic face of mast cell membranes, including the abundant immunoglobin E (IgE) receptor (FcεRI) and its signaling partners, has revealed that most (if not all) proteins in native membranes are distributed as small, dispersed clusters before stimulus (2,16,17). Despite this order, the membrane is adaptable and capable of dynamic reorganization. This is well illustrated by TEM observations showing that FcεRI can coalesce within minutes of activation into patches as large as 200–400 nm in diameter (2,16,17). Because these sites of receptor aggregation accumulate many signaling proteins, they are presumed to be sites of active signaling. The signaling patches typically occupy ''dark'' membrane regions that show enhanced labeling with osmium, indicating high levels of double bond-containing lipids and/or cholesterol (2), and are frequently bordered by coated pits (see Fig. 1 *B*). It is of great interest, therefore, to determine if the signaling patches are indeed distinct topographic features in mast cell membranes.

Here, we complement electron microscopy with atomic force microscopy (AFM) to further examine the topography of the cytoplasmic face of plasma membrane sheets stripped from tumor mast cells (rat basophilic leukemia RBL-2H3). AFM has been used extensively to characterize biological samples because it can be routinely performed in natural fluid environments, which is a clear advantage over vacuum conditions imposed by the TEM. It has also been well established that AFM can provide undistorted images of soft, compliant membrane structures, due in large part to sensitive

Submitted August 31, 2005, and accepted for publication December 14, 2005.
Address reprint requests to A. R. Burns, E-mail: aburns@sandia.gov.

0006-3495/06/04/2404/10 $2.00
doi: 10.1529/biophysj.105.073692

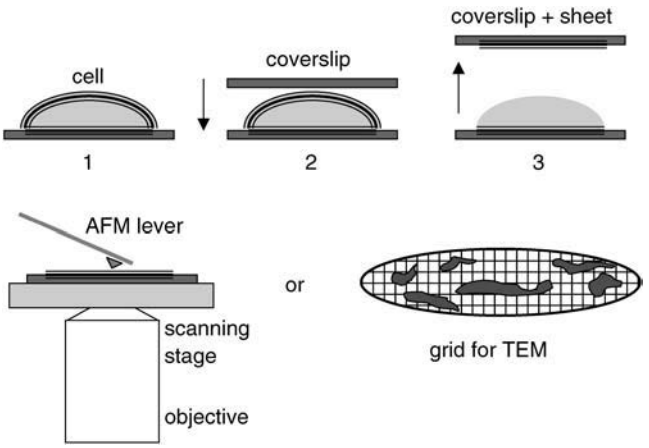

FIGURE 1 Schematic view of the membrane sheet preparation for AFM analysis. Whole cells are dispensed onto substrates (step *1*). A poly-L-lysine-coated coverslip is lowered (step *2*) onto the dorsal surface of lightly fixed cells to make a ''sandwich'' that can be separated (step *3*), producing a monolayer of membrane sheets, all oriented with the cytoplasmic face-up for simultaneous AFM/fluorescence imaging (*lower left*). A very similar procedure generates cytoplasmic face-up membrane sheets on nickel grids for TEM imaging (*lower right*).

force feedback detection and use of the tapping mode to reduce lateral forces (18–21). In model membrane studies, AFM has been able to map phase-separated lipid domains (22–24). A key feature of this study is the ability to correlate membrane topographic features with the locations of fluorescently tagged proteins and lipids through simultaneous acquisition of AFM and confocal fluorescence images (23,24).

Our AFM results show that the inner side of the plasma membrane is composed of numerous irregular-shaped raised domains that contain both resting and activated FcεRI, aggregated GM1, and clathrin. When present, a fibrous meshwork appears to link adjacent raised domains, suggesting a role for the cortical cytoskeleton in organizing these prominent features of the plasma membrane landscape. Taken together, the results identify the raised domains seen in AFM as the darkened membrane regions seen by TEM. Although the raised domains are likely to be heterogeneous in content, they importantly include sites of signaling and endocytosis.

MATERIALS AND METHODS

Antibodies and reagents

The dinitrophenol (DNP)-specific IgE was affinity purified from the ascitic fluid of mice bearing the H1 DNP-ε-26.82 hybridoma (25) and conjugated to Alexa 488 using a kit supplied by Molecular Probes (Eugene, OR). Monoclonal antibodies to anti-clathrin heavy chain were purchased from Calbiochem (San Diego, CA). Alexa-488-conjugated anti-mouse IgG $F(ab')_2$ and Alexa-488-conjugated recombinant cholera toxin B fragment (Alexa-488-CTX-B) were purchased from Molecular Probes. Monomeric perfringolysin O (PFO) was produced as His-tagged recombinant protein in *Escherichia coli* and purified by Ni-NTA affinity chromatography.

Cell culture and treatment

Stock cultures of RBL-2H3 mast cells were maintained in minimal essential medium (Gibco, Invitrogen, Carlsbad, CA) supplemented with 10% Hybrimax (Sigma, St. Louis, MO) and passaged twice weekly. Cells were dispensed into suspension dishes containing 15 mm diameter clean glass coverslips. In some cases, the cells were preincubated for 1 h with Alexa 488 IgE (2 μg/ml) to prime and label the FcεRI. Cells were then incubated for 7 min at 37°C, plus or minus polyvalent antigen (DNP-bovine serum albumin (BSA), 0.1 μg/ml), followed by fixation and sheet preparation (described below). For the GM1 study, cells were treated with Alexa 488 cholera toxin for 10 min at either room temperature (RT) or 37°C before fixation. For cholesterol depletion, cells were pretreated for 30 min with 10 μM methyl-β-cyclodextrin (MβCD) (Sigma) in MEM containing 10% fatty-acid-free BSA before fixation and sheet preparation.

Preparation of plasma membrane sheets for AFM/fluorescence

As shown schematically in Fig. 1, the cytoplasmic face of membrane sheets were prepared for simultaneous AFM/fluorescence imaging by modification of the procedure used for TEM imaging (16), described below, and originated by Sanan and Anderson (26). Ethanol-cleaned 25 mm diameter glass coverslips were glow discharged, coated with 0.2 mg/ml of poly-L-lysine for 30 min, rinsed in doubly distilled water for 10 s, and air dried. Cells were fixed in 0.5% paraformaldehyde in phosphate-buffered saline (PBS) in the presence of Hoechst 33942 nuclear stain for 7 min at RT, rinsed, and held in PBS. Next, the monolayer was dipped in HEPES buffer and inverted onto the center of a poly-L-lysine-coated coverslip, without applying pressure. The resulting ''sandwich'' was left for 10 min at RT on moist 4.25 cm filter paper then separated by floating apart in HEPES buffer. For the clathrin labeling experiment, coverslips carrying membrane sheets were incubated in mouse monoclonal anti-clathrin heavy chain for 30 min. This was followed by rinsing three times in PBS and incubation in the secondary antibody Alexa 488 $F(ab')_2$ goat anti-mouse IgG with a 0.1% solution of BSA for 30 min at room temperature. Coverslips were rinsed three times in PBS, mounted in a coverslip dish (Harvard Apparatus, Holliston, MA), and immediately immersed in PBS for imaging.

Plasma membrane sheet preparation and gold labeling for TEM

Plasma membrane sheets were prepared and processed for TEM as described in Wilson et al. (16) and shown schematically in Fig. 1. Briefly, coverslips of live or lightly fixed (0.5% paraformaldehyde for 10 min at 37°C) cells were immersed in ice-cold HEPES buffer (25 mM HEPES, pH 7, 25 mM KCl, 2.5 mM $Mg(C_2H_3O_3)_2$) and inverted onto nickel electron microscopy (EM) grids that had been coated with formvar and carbon and, on the day of the experiment, glow discharged and floated on poly-L-lysine (0.8 mg/ml for 30 min, followed by 10 s doubly distilled water rinse and air drying). Pressure was applied to the coverslip for 20 s by bearing down with a cork. The coverslips were lifted, leaving sections of the upper cell surface adherent to the poly-L-lysine-coated grid. Membranes were immediately fixed in 2% paraformaldehyde for 10 min at 4°C. FcεRI β-subunits were labeled from the inside sequentially with primary antibodies and gold-conjugated secondary reagents by inverting grids onto droplets. Cholesterol on the inner face of the plasma membrane was labeled using 5 nm colloidal gold (BBInternational, Cardiff, UK) conjugated to recombinant, monomeric PFO, using the manufacturer's instructions. Samples were postfixed in 2% glutaraldehyde in PBS, stained for 10 min with 1% OsO_4 prepared in 0.1 M cacodylate buffer, and washed 5 min with cacodylate buffer followed by doubly distilled water. Samples were finally processed for 10 min each in 1% aqueous tannic acid and 1% aqueous uranyl acetate, with intermediate and final washes in doubly distilled water. Grids were air dried and examined using a Hitachi 600 transmission electron microscope.

Simultaneous AFM and fluorescence imaging

The apparatus to obtain simultaneous AFM and confocal fluorescence imaging has been described in detail elsewhere (23,24). Briefly, an inverted microscope (Olympus IX70, Tokyo, Japan) was modified to accommodate a Bioscope AFM head (Veeco, Santa Barbara, CA). The coverslip dish containing membrane sheets was mounted onto an X-Y piezo scanner plate (Nanonics, Tel Aviv, Israel). The scanner plate in turn was mounted on a manual X-Y stage that allowed large range viewing of the sample with a Hg lamp. In this way, whole cells indicated by the Hoechst nuclear stain were detected and avoided. The AFM probe was centered on the membrane sheets, and the Hg lamp was extinguished. Excitation light from a 488 nm Ar^+ laser was focused by a 100×, numerical aperture 1.2 oil objective (Olympus) to a 300 nm spot and aligned with the AFM probe by visual inspection. (A slight nanometer-scale offset between fluorescence and AFM images can occur due to the alignment.) Epifluorescence was spatially filtered in a confocal manner by coupling into a 50 μm diameter core multimode fiber connected to an avalanche photodiode detector. AFM and fluorescence images were acquired with a single controller (RHK, with SPM32 software). All the AFM data presented here were acquired under forces <1 nN, with levers (Olympus TR400-PSA, nominal force constant of 0.08 N/M) in tapping mode. The XY scanner plate was calibrated with a 463 nm square grid grating (Ted Pella, Redding, CA), and the AFM head was calibrated in Z with known 25.5 nm steps (TGZ01, NT-MDT Mikromasch, Allen, TX). Three-dimensional (3-D) rendering was accomplished using WSXM freeware (Nanotec, Madrid, Spain).

Analysis of AFM topography

Specific features in the AFM topography were analyzed by line profiling routines provided in WSXM and SPM32 imaging software (see Fig. 7 for examples). Each line profile gave both height and width information. The heights of raised domains are measured relative to the surrounding membrane (not relative to the substrate). Since raised domains were irregularly shaped, care was taken for each domain to acquire representative profiles. All the representative height and width data were entered into KaleidaGraph software (Synergy Software, Reading, PA) for statistical analysis (Table 1) and histogram binning (see Fig. 9).

RESULTS AND DISCUSSION

Aggregated receptors are found in raised domains

As shown previously (2,16,17), TEM imaging of immunogold-labeled IgE receptors, FcεRI, in RBL membrane sheets reveals recruitment to electron-dense dark patches upon activation. The dark patches preexist in resting cells but become more prominent with FcεRI clustering. In Fig. 2 *A*, IgE-primed receptors are distributed across the resting membrane in small clusters. Clathrin lattices (*arrow*) and clathrin-coated pits are features of the resting membrane. Upon activation by the addition of multivalent antigen (Fig. 2 *B*), FcεRI form large clusters that localize to the characteristic dark patches. Clathrin lattices and clathrin-coated pits are seen inside and in close proximity to the dark patches. Budding pits often contain the IgE receptors after activation, indicating that dark contrast regions are involved in both signaling and endocytosis (2). Prior work also showed that GM1 is recruited independently to the same dark patches containing activated FcεRI, after its CTX-B aggregation (2). Thus activated FcεRI, aggregated GM1, and clathrin colocalize in the dark patches.

TABLE 1 Topographic information

Structure (No. of measurements)	Domain height (nm)	Domain width (nm)
	±Standard deviation	±Standard deviation
Flat region of membrane* (5)	7.0 ± 0.2	–
Flat region of membrane* (5) Treated with MβCD	6.8 ± 0.7	–
Raised domain, activated (68)	50 ± 16	575 ± 315
Raised domain, resting (38)	43 ± 13	394 ± 191
Raised domain, activated (34) Treated with MβCD	36 ± 17	650 ± 354
Raised domain, resting (46) Treated with MβCD	24 ± 9	358 ± 244

*Relative to poly-L-lysine covered substrate.

We began our simultaneous AFM/confocal fluorescence imaging of resting and activated RBL-2H3 mast cell sheets with the objective of observing any topographically distinct membrane features that contained fluorescence-tagged FcεRI IgE receptor. Our technique of membrane harvesting, shown schematically in Fig. 1, exposes only the cytoplasmic surface to AFM imaging. However, either surface can be labeled with a fluorescent tag. Thus in the first experiments, the cells were primed with Alexa-488-conjugated anti-DNP IgE to occupy the high affinity IgE receptors that are present on the extracellular surface at levels approaching 200,000/cell. This priming step provides a fluorescence tag for receptor tracking but does not induce signaling responses.

The results for resting and activated cells are shown in Fig. 3, *A–F*. AFM topographic images of the cytoplasmic surface of resting membrane sheets reveal raised domains (Fig. 3 *A*, *arrows*). The edge of the membrane sheet can also be seen. In the resting sheets, the simultaneous fluorescence image (Fig. 3 *B*) exhibits semiuniform fluorescence; however, occasional large clusters can be resolved (*white arrows*, Fig. 3 *B*). These data are consistent with dispersed clusters of resting FcεRI, containing only a few receptors, that are below the resolution of the confocal microscope (~300 nm). We do see, however, that bright regions (*white arrows*) within the uniform fluorescence map to the raised domains in the AFM topography (Fig. 3 *A*). To accentuate the correlation, we have used edge-finding routines in Adobe Photoshop (Adobe Systems, San Jose, CA) to overlay the domain boundaries on the fluorescence image (Fig. 3 *C*). After activation induced by cross-linking IgE-bound receptors with the polyvalent ligand DNP-BSA, we clearly see raised domains in the AFM topography of the membrane sheets (Fig. 3 *D*). Moreover, the semiuniform fluorescence observed in the resting sheets gives way to strongly clustered, bright foci of FcεRI in the activated sheets (Fig. 3 *E*). The strong clustering correlates precisely with the raised domains in the topography (Fig. 3 *F*).

Cross-linked gangliosides redistribute to raised domains

Since prior TEM work showed that GM1 aggregated by CTX-B fragments is recruited independently to the same

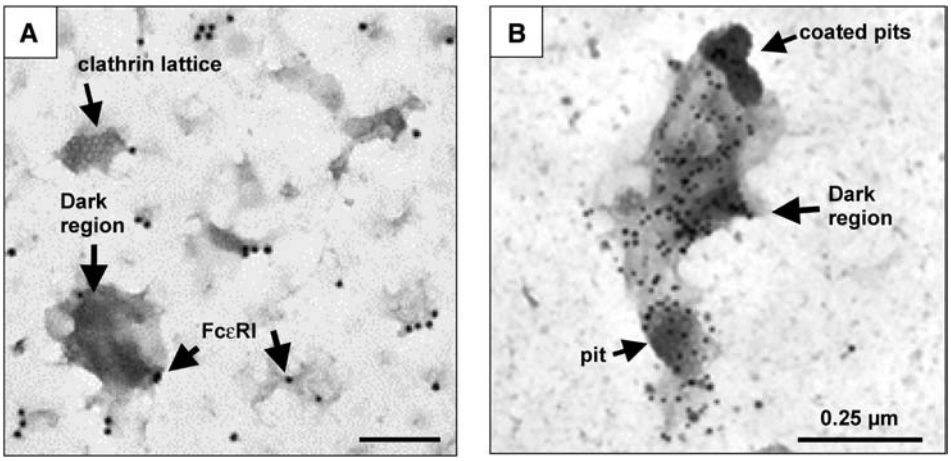

FIGURE 2 TEM images of FcεRI IgE receptor distributions in membrane sheets, as revealed by 10 nm anti-FcεRI β-gold labels. The membranes were prepared from IgE-primed cells, without (*A*) or with (*B*) 5 min of antigen (DNP-BSA) activation. Immunogold labeling is performed after membrane harvesting. In resting membranes (*A*), the receptor is distributed uniformly in small clusters. In activated cells (*B*), it forms large clusters localized in dark regions. Clathrin-coated pits are visible and tend to occur on the edges of the dark regions.

dark patches containing cross-linked FcεRI (2), we checked to see if cross-linked GM1 is present in the raised domains. In this case, we incubated live, resting RBL-2H3 cells with Alexa-488-conjugated CTX-B before sheet preparation. As shown in Fig. 4, *A* and *B*, raised domains in the AFM topographic image (Fig. 4 *A*) in the resting membrane sheets do indeed correlate with bright clusters of GM1 stained with labeled CTX-B (Fig. 4 *B*). This correlation is made clear in

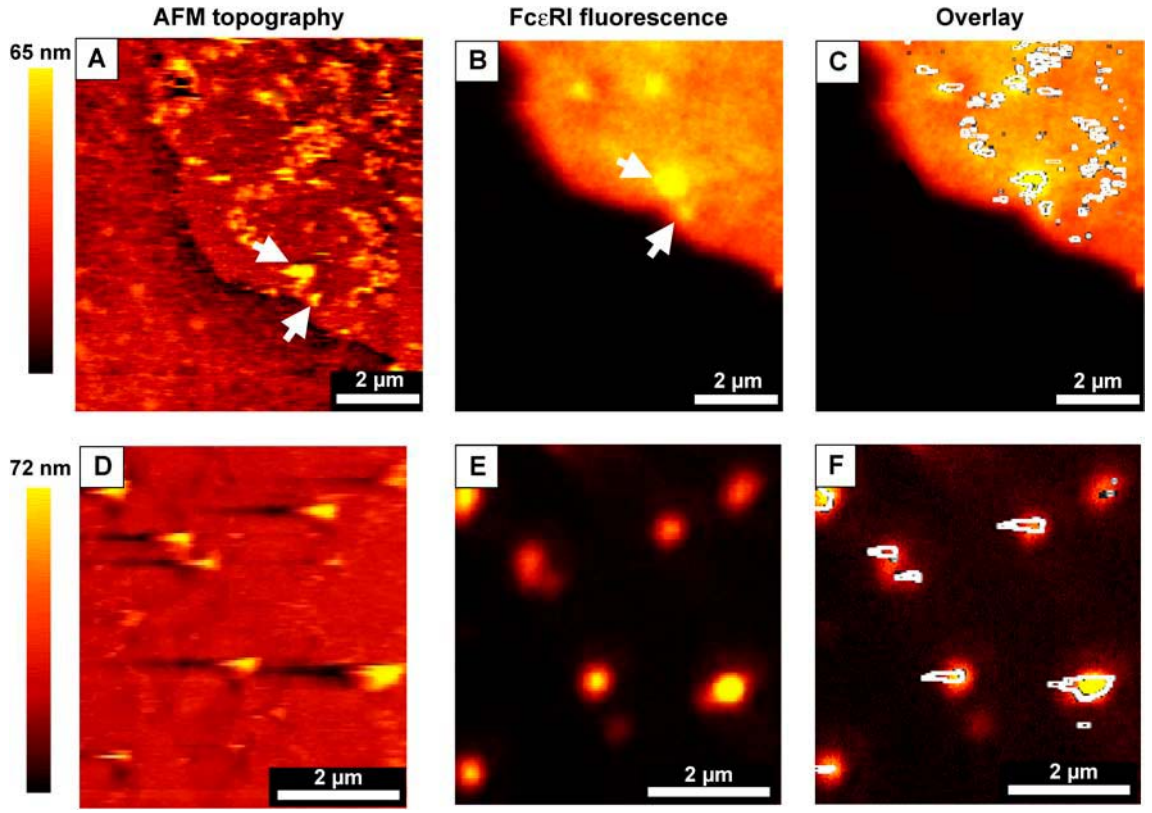

FIGURE 3 Simultaneous AFM and confocal fluorescence images of FcεRI IgE receptor distributions in membrane sheets. The membranes were prepared from Alexa-488-labeled IgE-primed cells, without (*A–C*) or with (*D–F*) 5 min of antigen (DNP-BSA) activation. In the resting membrane (*A–C*), the white arrows point to examples of correlation between bright fluorescent IgE spots (*B*) marking small clusters of resting receptors near the edge of the membrane sheet that correlate with raised domains in the AFM image (*A*). In *C*, we have overlaid the topographic domain edges from *A* onto the fluorescence image (*B*) to confirm that the tagged IgE receptors cluster in ''raised'' membrane regions. The clustering is much more pronounced for activated receptors (images *D* and *E*), where the bright regions in the IgE fluorescence (*E*) map clearly with the raised domains in the AFM image (*D*). In *F*, we have overlaid the topographic domain edges from *D* onto the fluorescence image (*E*) to confirm the coincidence of receptors and raised domains. The pseudocolor scales indicate the relative height of membrane features in the AFM images (*A* and *D*).

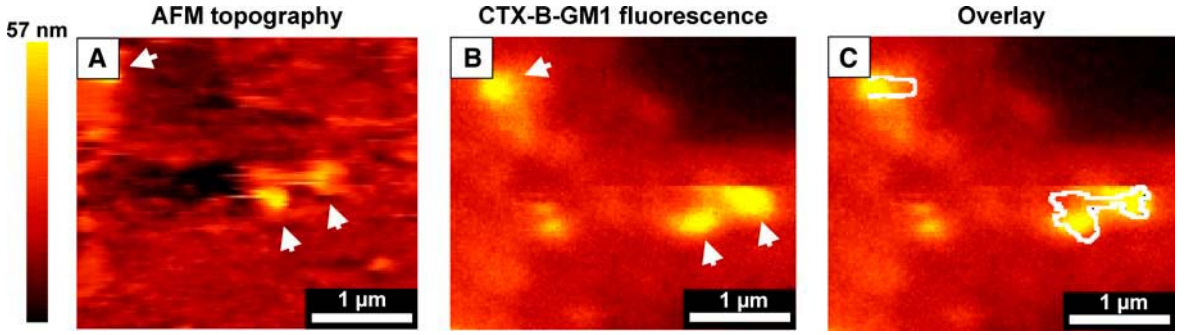

FIGURE 4 Simultaneous AFM (*A*) and confocal fluorescence (*B*) images of resting RBL cell membrane sheets where the GM1 ganglioside is aggregated by Alexa-488-labeled CTX-B before fixation. In *B*, the upper right corner is dark due to photobleaching. Arrows in the paired images point to examples of correlation between fluorescent label in *B* and raised domains in *A*. In *C*, we have overlaid the topographic domain edges from *A* onto the fluorescence image (*B*) to confirm the colocalization. The pseudocolor scale indicates the relative height of membrane features in the AFM image (*A*).

the overlay (Fig. 4 *C*). In contrast, there was no correlation between fluorescence and AFM topographic features when Alexa-488-cholera toxin was applied to prefixed cells (not shown). The latter is consistent with the essentially random distribution of GM1 observed in TEM for prefixed cells (2) and supports the concept that there are distinct membrane features on the cytoplasmic face associated with the RBL signaling patches.

Clathrin-coated vesicles bud from raised domains

Previous TEM studies (2,16) have shown that clathrin-coated vesicles tend to bud from the dark patches in membrane associated with FcεRI signaling (see pits marked with *arrows* in Fig. 2 *B*). To access the relationship of clathrin to the raised domains on the cytoplasmic surface that are observed with AFM, membrane sheets were treated with monoclonal antibodies to clathrin heavy chain, followed by labeling with fluorescent anti-mouse antibodies. The results are shown in Fig. 5. Once again, there is a very good correlation between raised domains (Fig. 5 *A*) and the distribution of clathrin (Fig. 5 *B*). Thus it is clear that the raised domains contain clathrin-coated pits. Occasionally, it is possible to resolve domed structures within large, irregularly shaped raised domains. This can be seen in Fig. 6, *A* and *B*, where Fig. 6 *B* is an expanded 3-D view of such a feature present in Fig. 6 *A*. One possible interpretation of the peaks in the 3-D view is that clathrin-coated vesicles are budding from a larger raised domain.

To summarize our results so far, we have seen raised domains in all the AFM topographic images of the membrane sheets (both resting and activated). All the raised domains appear to label with IgE receptor, GM1 that has been aggregated by CTX-B, and clathrin. Since all three are known from the TEM results (2,16,17) to colocalize in the dark patches, particularly for the activated cells, it is straightforward to conclude that the dark patches correspond to the raised domains in AFM topography and represent distinct topographic feature of these membranes.

Repeated measurements discussed in detail below, and summarized in Table 1 and Fig. 9, reveal that the height of the raised domains, relative to the surrounding membrane,

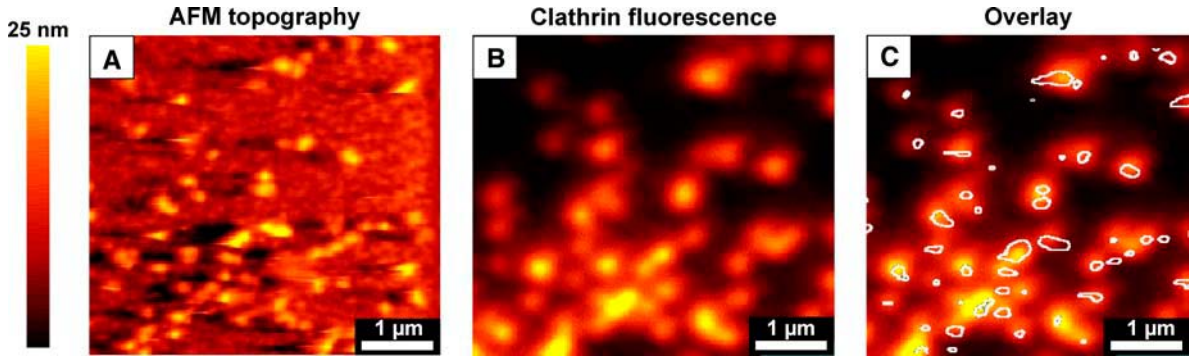

FIGURE 5 Simultaneous AFM (*A*) and confocal fluorescence (*B*) images of resting RBL cell membrane sheets where clathrin is labeled with mouse monoclonal anti-clathrin heavy chain and Alexa 488 $F(ab')_2$ goat anti-mouse IgG. The raised domains in *A* correlate strongly with the bright regions in *B*, thus clearly indicating the presence of clathrin. In *C*, we have overlaid the topographic domain edges from *A* onto the fluorescence image (*B*) to confirm the colocalization. The pseudocolor scale indicates the relative height of membrane features in the AFM image (*A*). In this particular sheet, the raised domains are reduced in height by treatment with 10 μM MβCD (see Fig. 7).

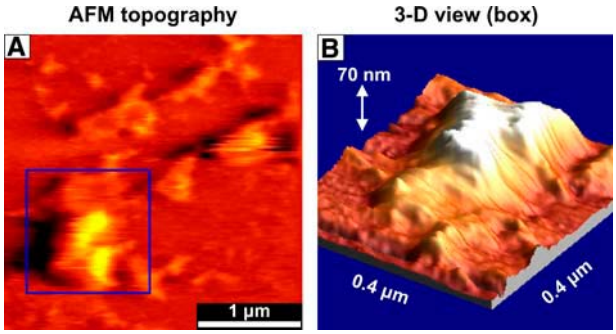

FIGURE 6 (*A*) AFM image at higher resolution of a resting RBL cell membrane sheet (clathrin labeled) showing several raised domains. (*B*) One domain (0.4 μm box) was selected for 3-D representation to highlight possible clathrin pits within the domain.

ranges from 15 nm to as much as 90 nm. By comparison, the flatter regions of these native membranes between the domains have an average thickness of ~7 nm, measured relative to the poly-L-lysine-coated substrate. (The edge of a membrane can be seen in Fig. 3 *A*.) This is not much greater than the 4.5 nm thickness of a typical model lipid bilayer (27) and is comparable to the 6.3 nm thickness measured for protein-containing ''purple membranes'' of *Halobacterium salinarum* (21). Thus the raised domains are significant protrusions that are much larger than the overall membrane thickness.

Cholesterol depletion reduces the height of raised domains

Cholesterol is a key component of the plasma membrane (28) and its loss has profound effects, including changes in recovery of specific components in light fractions of sucrose density gradient used as a biochemical measure of membrane raft integrity. Cholesterol depletion prohibits the formation of coated pits (29), leaving the membrane studded with flat clathrin arrays (*arrow*, Fig. 7 *D*) that cannot deliver cargo to the cell interior. Membrane perturbations associated with cholesterol depletion have frequently been used as an indicator of raft involvement (30,31). To determine the effects of cholesterol depletion on the topography of the cytoplasmic face, we incubated RBL cells with 10 μM MβCD for 30 min at 37°C before fixing cells and preparing membrane sheets for AFM measurements. Representative results in Fig. 7 demonstrate that the height of the raised domains on RBL membrane sheets is markedly reduced by cholesterol depletion. When analyzed in line profile or cross section (*red lines* in Fig. 7, *A* and *B*), a representative raised domain in control membranes has a peak height of almost 70 nm. By comparison, cross sectional analysis of a representative raised domain in a cholesterol-depleted membrane has a peak height of only 20 nm (*black lines* in Fig. 7, *A* and *C*). Analyses of repeated measurements are summarized in Table 1 and Fig. 9. Importantly, the loss of cholesterol fails to significantly alter the 7 nm thickness of the flat regions of membrane.

Cholesterol is observed in TEM dark patches

In prior work, x-ray spectral analysis of dried membrane sheets indicated that the dark patches have higher levels of carbon than bulk membrane (2). This result suggested that they contain a higher density of proteins and associated lipids and/or cholesterol than the surrounding membrane.

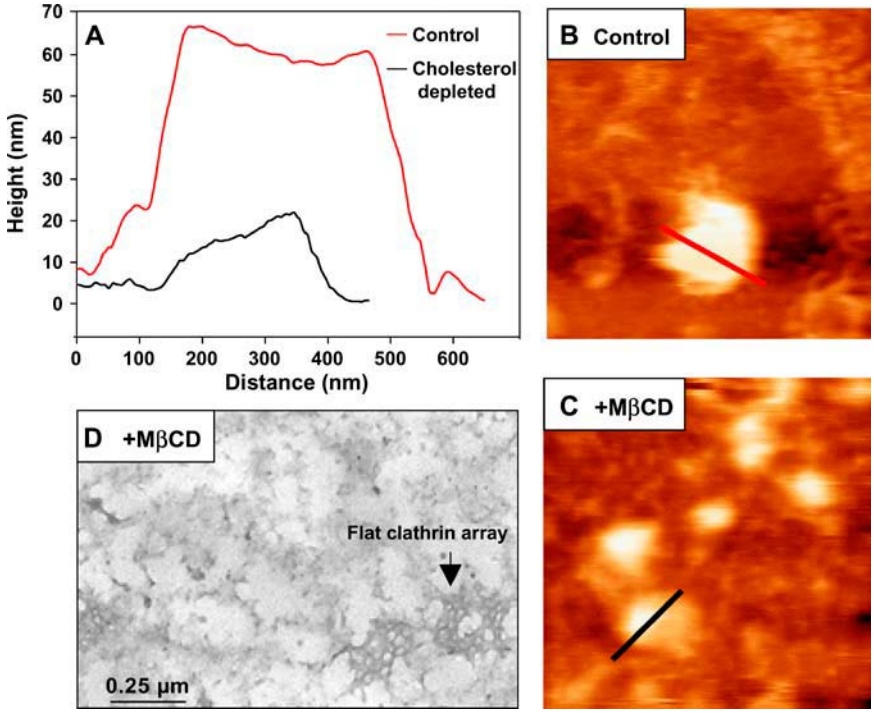

FIGURE 7 (*A*) Example of AFM topographic line profiles of raised domains for both control RBL cell membrane sheets (*B*) and those treated with 10 μM MβCD (*C*). The measurements show that the height of individual domains is substantially lower in cholesterol-depleted membranes (*black line*) than in control membranes (*red line*). The data for all the sheets studied are summarized in Table 1 and in histograms of Fig. 9. The data are independent of labeling. Image *B* was from a resting cell and image *C* was from an activated cell. A representative TEM image of cholesterol-depleted membranes is shown in *D*, where ''flattened'' clathrin arrays can be observed.

Fig. 8 shows two TEM images that support the concept that cholesterol is an important component of the dark patches and is thus in good agreement with their coidentity with the cholesterol-sensitive raised regions seen by AFM. In Fig. 8, *A* and *B*, membrane sheets from control and MβCD-treated cells were labeled with 5 nm gold particles coated with a monomeric form of PFO (32). A toxin produced by *Clostridium perfringens*, PFO specifically binds cholesterol and has been successfully used as a cytochemical probe for electron microscopy (33). In the control cells (Fig. 8 *A*), cholesterol is present in bulk membrane but is markedly clustered in a large darkened region (*arrow*, *lower left*). There is very little label in the MβCD-treated (cholesterol-depleted) cells (Fig. 8 *B*). Thus the dark patches contain high levels of cholesterol as well as proteins.

Quantifying the dimensions of the raised regions

The data above show that raised domains are a consistent feature of all the membrane sheet preparations studied by AFM to date. In Fig. 9, eight normalized histograms provide an expanded analysis of the raised domain heights and widths. The height and width data are broken down into activated and resting and with and without the MβCD treatment that extracts cholesterol. The histogram data are also condensed in Table 1, which includes the number of measurements for each structure. We see an increase in both the heights and widths of the raised domains for activated cells relative to resting cells. This is consistent with TEM observations (2,16,17) of protein recruitment to the dark patches. We see the same trend after MβCD treatment, which reduces the height of all raised domains but does not appear to reduce domain widths. It is important to note that concerning domain widths, the skewed histograms and large ranges are most likely due to aggregates of smaller domains. This would also reduce correlation, if any, between height and widths.

We note that these measurements were made using sheets labeled with IgE alone and also with sheets exposed to DNP-BSA and CTX-B on the extracellular side and with Abs to clathrin on the cytoplasmic side. To address the concern that these various labels would add substantial thickness to the membranes, we compared domain heights between membranes from resting cells that were unprimed with IgE relative to those that were and between membranes from activated cells that were labeled with primary and secondary antibodies for clathrin relative to those that were not. We found no statistical difference in the height of resting cells that were unprimed with IgE relative to those that were. We found that the clathrin labels added no more than 13 ± 5 nm to the domain height. In short, we attribute the domain heights to protein clustering and associated cholesterol and very little, if any, to the labels.

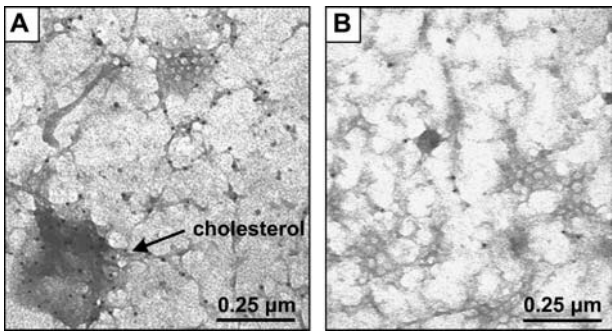

FIGURE 8 Distribution of PFO conjugated to 5 nm gold nanoparticles on RBL cell membrane sheets seen by TEM. On sheets from control cells (*A*), the abundant PFO label associates preferentially, but not exclusively, with darkened membrane (*arrow*). After treatment with 10 μM MβCD (*B*), only a few gold particles remain, demonstrating specificity of the PFO binding.

Linking raised domains to the cytoskeleton

The relationship between membrane signaling domains and the cytoskeleton is of great interest (34). Diffusion confinement zones have been attributed to the cytoskeleton (35,36). In the mast cell membrane, the cortical cytoskeleton forms a continuous submembranous meshwork (37). This meshwork is frequently observed on the inner surface of native membrane sheets in TEM images, where it seems to connect the darkened membrane areas (Fig. 10 *C;* also Fig. 8 *A*). Previous studies showed that the fibers bind phalloidin-gold particles and thus contain F-actin (16). When imaged by the AFM (Fig. 10, *A* and *B*), similar networks of fibers (*white arrows*) can be seen to surround and connect the raised domains. This supports the concept that the topography of the inner membrane is organized in part by the cortical cytoskeleton. We note that the cytoskeletal fibers are not seen in every AFM or TEM image of membrane sheets, whereas conventional thin section TEM shows a continuous actin meshwork under the mast cell membrane (37). Thus it is likely that a variable degree of cytoskeletal disassembly occurs during the membrane sheet preparation.

SUMMARY AND CONCLUSIONS

We have used simultaneous AFM and confocal fluorescence imaging of the cytoplasmic surface of membranes stripped from both resting and activated RBL-2H3 cells to reveal the presence of distinct membrane features (raised domains) that have the ability to concentrate numerous membrane molecules, including cross-linked receptors, gangliosides, and clathrin. Raised domains are found in the membrane of both resting and activated cells. The principal effect of cell activation is to cause the reorganization of membrane components into larger domains. Based upon AFM measurements of their thickness, lipid phase changes are unlikely to contribute substantially to these raised domains. We suggest instead that they represent areas that concentrate transmembrane and peripheral membrane proteins, either constitutively or inducibly, and that their bulky cytoplasmic tails and associated binding partners contribute to the height. Another significant

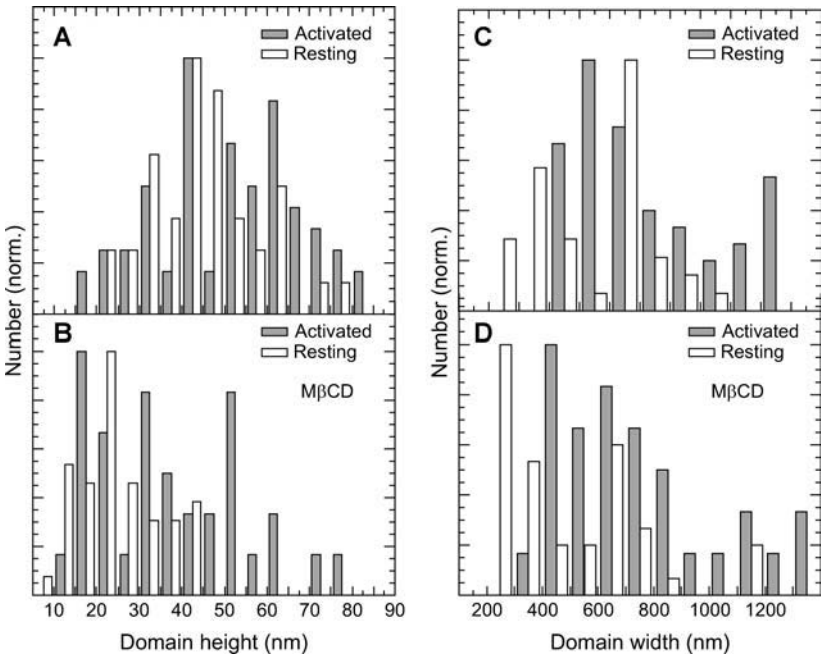

FIGURE 9 Histogram display of distributions of raised domain heights and widths as measured by cross section (illustrated in Fig. 7). The data incorporate all the membrane sheets in this study and were independent of cell labeling by IgE, CTX-B, or clathrin. The clathrin label (mouse monoclonal anti-clathrin heavy chain and Alexa 488 $F(ab')_2$ goat anti-mouse IgG) adds ~13 nm to the domain height. Histogram *A*(*C*) shows the distribution of domain heights(widths) for activated (*shaded bars*) and resting (*open bars*) membrane sheets. Histogram *B*(*D*) is the distribution of heights(widths) for membranes subjected to cholesterol extraction by MβCD.

contributor to the thickness may be clathrin lattices and clusters of clathrin-coated pits.

Based on composition, we conclude that the raised domains seen by AFM correspond to the dark patches observed in TEM images of signaling domains that also localize the immunoreceptor, FcεRI, at least 10 associated signaling molecules, and also molecules involved in coated pit assembly to dark regions of activated mast cell membranes (16,17). Concentrated proteins could explain in part the increased amount of carbon found by x-ray spectral imaging in the darkened patches (2).

We showed by TEM that the cholesterol marker PFO preferentially binds darkened membranes and by AFM that cholesterol extraction by MβCD causes a large reduction in height of the raised domains. These complementary results indicate that cholesterol contributes significantly to the formation or stability of the raised domains. The mechanism is not known with certainty. It is possible that MβCD reduces domain height by extracting not only cholesterol but also proteins in the form of protein-cholesterol complexes. Another possibility is that the recruitment of signaling proteins to the domains is reduced in the absence of cholesterol. Additionally, we have observed by EM that the inner membrane of MβCD-treated cells is enriched in flat clathrin arrays but is totally lacking in coated vesicles (Fig. 7 *D*). If much of the height is due to the curvature of 3-D clathrin lattices, cholesterol extraction would appear to ''flatten'' those structures.

The apparent relationship of the raised domains to the cytoskeleton (Fig. 10) is of particular interest. Previous fluorescence recovery after photobleaching data (38) and SPT data (35,36) have led to models that consider roles for cytoskeletal ''fences'' or ''corrals'' and anchored protein ''pickets'' in the temporary, dynamic confinement of membrane proteins and lipids and also in the formation of less mobile macromolecular complexes during signaling. In particular, the SPT studies typically reveal free diffusion of proteins and lipids within 40–700 nm confinement zones accompanied by infrequent intercompartmental transitions (''anomalous diffusion'', ''hop diffusion''). However, particularly for particles linked

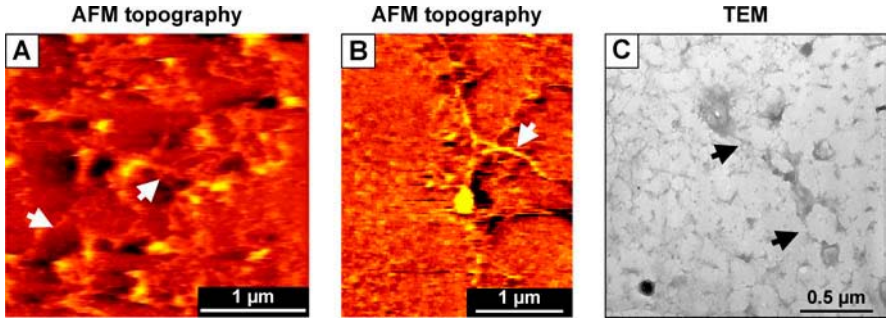

FIGURE 10 (*A* and *B*) AFM topography of RBL cell membrane sheets where cytoskeleton cables (*white arrows*) appear to link numerous raised domains. The maximum height in *A* is 54 nm and the maximum height in *B* is 45 nm. (*C*) Cytoskeleton cable linkages (*black arrows*) appear in a TEM image.

to lipids, it has never been clear why interactions of the cytoskeleton with components of the inner leaflet of the membrane bilayer would regulate mobility in the outer leaflet of the bilayer. The AFM images presented here show cytoskeletal elements surrounding and connecting the raised domains. These images thus raise the possibility that the cortical cytoskeleton may determine the stability and characteristics of membrane domains, which in turn may determine the ability of proteins (and lipids) to access and escape from these specialized regions.

In summary, AFM/fluorescence imaging of the inner membrane landscape has revealed levels of topographical complexity that are not addressed either in the well-mixed lipid and protein model proposed by Singer and Nicholson (1) or in progressively more complex models developed over the subsequent decades that incorporate concepts of compositional and functional heterogeneity within the membrane bilayer and between the membrane and the cytoskeleton (34). Further analysis of the composition of distinct membrane compartments across the topographic landscape is expected to reveal new insight into the relationship of membrane geometry to membrane molecular organization and function.

Sandia is a multi-program laboratory operated by Sandia Corporation, a Lockheed Martin Company, for the U.S. Dept. of Energy under contract DE-AC04-94AL85000. Use of the electron microscopy facilities at the University of New Mexico-Health Sciences Center is gratefully acknowledged.

This work was supported in part by National Institutes of Health grants P20GM66283, R01GM49814, and R01AI051575 and in part by the Division of Materials Science, Office of Basic Energy Sciences, U.S. Dept. of Energy.

REFERENCES

1. Singer, S., and G. Nicolson. 1972. The fluid mosaic model of the structure of cell membranes. *Science*. 175:720–731.
2. Wilson, B., S. Steinberg, K. Liederman, J. Pfeiffer, Z. Surviladze, J. Zhang, L. Samelson, L. Yang, P. Kotula, and J. Oliver. 2004. Markers for detergent-resistant lipid rafts occupy distinct and dynamic domains in native membranes. *Mol. Biol. Cell*. 15:2580–2592.
3. Oliver, J., and R. Berlin. 1982. Mechanisms that regulate the structural and functional architecture of cell surfaces. *Int. Rev. Cytol*. 74:55–94.
4. Jacobson, K., E. Sheets, and R. Simson. 1995. Revisiting the fluid mosaic model of membranes. *Science*. 268:1441–1442.
5. Lai, E. 2003. Lipid rafts make for slippery platforms. *J. Cell Biol*. 162: 365–370.
6. Edidin, M. 2003. The state of lipid rafts: from model membranes to cells. *Annu. Rev. Biophys. Biomol. Struct*. 32:257–283.
7. Edidin, M. 2001. Shrinking patches and slippery rafts: scales of domains in the plasma membrane. *Trends Cell Biol*. 11:492–496.
8. Brown, D., and E. London. 1998. Functions of lipid rafts in biological membranes. *Annu. Rev. Cell Dev. Biol*. 14:111–136.
9. Field, K., D. Holowka, and B. Baird. 1995. FcεRI-mediated recruitment of p53/56^{lyn} to detergent-resistant membrane domains accompanies cellular signaling. *Proc. Natl. Acad. Sci. USA*. 92:9201–9205.
10. Koumanov, K., C. Tessier, A. Momchilova, C. Rainteau, C. Wolf, and P. Quinn. 2005. Comparative lipid analysis and structure of detergent-resistant membrane raft fractions isolated from human and ruminant erythrocytes. *Arch. Biochem. Biophys*. 434:150–158.
11. Douglass, A., and R. Vale. 2005. Single-molecule microscopy reveals plasma membrane microdomains created by protein-protein networks that exclude or trap signaling molecules in T cells. *Cell*. 121:937–950.
12. Friedrichson, T., and T. Kurzchalia. 1998. Microdomains of GPI-anchored proteins in living cells revealed by crosslinking. *Nature*. 394: 802–805.
13. Varma, R., and S. Mayor. 1998. GPI-anchored proteins are organized in submicron domains at the cell surface. *Nature*. 394:798–801.
14. Pralle, A., P. Keller, E. Florin, K. Simons, and J. Horber. 2000. Sphingolipid-cholesterol rafts diffuse as small entities in the plasma membrane of mammalian cells. *J. Cell Biol*. 148:997–1007.
15. Prior, I., C. Muncke, R. Parton, and J. Hancock. 2003. Lipid rafts: heterogeneity on the high seas. Direct visualization of Ras proteins in spatially distinct cell surface microdomains. *J. Cell Biol*. 160: 165–170.
16. Wilson, B., J. Pfeiffer, and J. Oliver. 2000. Observing FcεRI signaling from the inside of the mast cell membrane. *J. Cell Biol*. 149:1131–1142.
17. Wilson, B., J. Pfeiffer, Z. Surviladze, E. Gaudet, and J. Oliver. 2001. High resolution mapping reveals distinct FcεRI and LAT domains in activated mast cells. *J. Cell Biol*. 154:645–658.
18. Müller, D., D. Fotiadis, and A. Engel. 1998. Mapping flexible protein domains at subnanometer resolution with the atomic force microscope. *FEBS Lett*. 430:105–111.
19. Müller, D., J. Heymann, F. Oesterhelt, C. Möller, H. Gaub, G. Büldt, and A. Engel. 2000. Atomic force microscopy of native purple membrane. *Biochim. Biophys. Acta*. 1460:27–38.
20. Czajkowsky, D., and Z. Shao. 1998. Submolecular resolution of single macromolecules with atomic force microscopy. *FEBS Lett*. 430: 51–54.
21. Stark, M., C. Möller, D. Müller, and R. Guckenberger. 2001. From images to interactions: high resolution phase imaging in tapping-mode atomic force microscopy. *Biophys. J*. 80:3009–3018.
22. Dufrêne, Y., W. Barger, J.-B. Green, and G. Lee. 1997. Nanometer-scale surface properties of mixed phospholipid monolayers and bilayers. *Langmuir*. 13:4779–4784.
23. Burns, A. 2003. Domain structure in model membrane bilayers investigated by simultaneous atomic force microscopy and fluorescence imaging. *Langmuir*. 19:8358–8363.
24. Burns, A., D. Frankel, and T. Buranda. 2005. Local mobility in lipid domains of supported bilayers characterized by atomic force microscopy and fluorescence correlation spectroscopy. *Biophys. J*. 89:1081–1093.
25. Liu, F., J. Bohn, E. Ferry, C. Yamamoto, C. Molinaro, L. Sherman, N. Klinman, and D. Katz. 1980. Monoclonal dinitrophenyl-specific murine IgE antibody–preparation, isolation, and characterization. *J. Immunol*. 6:2728–2737.
26. Sanan, D., and R. Anderson. 1991. Simultaneous visualization of LDL receptor distribution and clathrin lattices on membranes torn from the upper surface of cultured cells. *J. Histochem. Cytochem*. 39:1017–1024.
27. Nagle, J., and J. Tristam-Nagle. 2000. Structure of lipid bilayers. *Biochim. Biophys. Acta*. 1469:159–195.
28. Maxfield, F., and D. Wustner. 2002. Intracellular cholesterol transport. *J. Clin. Invest*. 110:891–898.
29. Subtil, A., I. Gaidarov, K. Kobylarz, M. Lampson, J. Keen, and T. McGraw. 1999. Acute cholesterol depletion inhibits clathrin-coated pit budding. *Proc. Natl. Acad. Sci. USA*. 96:6775–6780.
30. Lawrence, J., D. Saslowsky, J. Edwardson, and R. Henderson. 2003. Real-time analysis of the effects of cholesterol on lipid raft behavior using atomic force microscopy. *Biophys. J*. 84:1827–1832.
31. Romanenko, V., Y. Fang, F. Byfield, A. Travis, C. Vandenberg, G. Rothblat, and I. Levitan. 2004. Cholesterol sensitivity and lipid raft targeting of Kir2.1 channels. *Biophys. J*. 87:3850–3861.

32. Ramachandran, R., R. Tweten, and A. Johnson. 2005. The domains of a cholesterol-dependent cytolysin undergo a major FRET-detected rearrangement during pore formation. *Proc. Natl. Acad. Sci. USA.* 102: 7139–7144.

33. Fujimoto, T., M. Hayahi, M. Iwamoto, and Y. Ohnoiwashita. 1997. Crosslinking plasmalemmal cholesterol is sequestered to caveolae: analysis with a new cytochemical probe. *J. Histochem. Cytochem.* 45: 1197–1205.

34. Vereb, G., J. Szöllosi, J. Matkó, P. Nagy, T. Farkas, L. Vígh, L. Mátyus, and T. Waldmann. 2003. Dynamic, yet structured: the cell membrane three decades after the Singer-Nicolson model. *Proc. Natl. Acad. Sci. USA.* 100:8053–8058.

35. Dietrich, C., B. Yang, T. Fujiwara, A. Kusumi, and K. Jacobson. 2002. Relationship of lipid rafts to transient confinement zones detected by single particle tracking. *Biophys. J.* 82:274–284.

36. Murase, K., T. Fujiwara, Y. Umemura, K. Suzuki, R. Iino, H. Yamashita, M. Saito, H. Murakoshi, K. Ritchie, and A. Kusumi. 2004. Ultrafine membrane compartments for molecular diffusion as revealed by single molecule techniques. *Biophys. J.* 86:4075–4093.

37. Pfeiffer, J., G. Deanin, J. Seagrave, B. Davis, and J. Oliver. 1985. Membrane and cytoskeletal changes associated with IgE-mediated serotonin release in rat basophilic leukemia cells. *J. Cell Biol.* 101:2145–2155.

38. Tang, Q., and M. Edidin. 2003. Lowering the barriers to random walks on the cell surface. *Biophys. J.* 84:400–407.